Precision Measurement of the Neutron Spin Asymmetry A_1^n and Spin-Flavor Decomposition in the Valence Quark Region

X. Zheng,[13] K. Aniol,[2] D. S. Armstrong,[22] T. D. Averett,[8,22] W. Bertozzi,[13] S. Binet,[21] E. Burtin,[17] E. Busato,[16] C. Butuceanu,[22] J. Calarco,[14] A. Camsonne,[3] G. D. Cates,[21] Z. Chai,[13] J.-P. Chen,[8] Seonho Choi,[20] E. Chudakov,[8] F. Cusanno,[7] R. De Leo,[7] A. Deur,[21] S. Dieterich,[16] D. Dutta,[13] J. M. Finn,[22] S. Frullani,[7] H. Gao,[13] J. Gao,[1] F. Garibaldi,[7] S. Gilad,[13] R. Gilman,[8,16] J. Gomez,[8] J.-O. Hansen,[8] D.W. Higinbotham,[13] W. Hinton,[15] T. Horn,[11] C.W. de Jager,[8] X. Jiang,[16] L. Kaufman,[12] J. Kelly,[11] W. Korsch,[10] K. Kramer,[22] J. LeRose,[8] D. Lhuillier,[17] N. Liyanage,[8] D. J. Margaziotis,[2] F. Marie,[17] P. Markowitz,[4] K. McCormick,[9] Z.-E. Meziani,[20] R. Michaels,[8] B. Moffit,[22] S. Nanda,[8] D. Neyret,[17] S. K. Phillips,[22] A. Powell,[22] T. Pussieux,[17] B. Reitz,[8] J. Roche,[22] R. Roche,[5] M. Roedelbronn,[6] G. Ron,[19] M. Rvachev,[13] A. Saha,[8] N. Savvinov,[11] J. Singh,[21] S. Širca,[13] K. Slifer,[20] P. Solvignon,[20] P. Souder,[18] D. J. Steiner,[22] S. Strauch,[16] V. Sulkosky,[22] A. Tobias,[21] G. Urciuoli,[7] A. Vacheret,[12] B. Wojtsekhowski,[8] H. Xiang,[13] Y. Xiao,[13] F. Xiong,[13] B. Zhang,[13] L. Zhu,[13] X. Zhu,[22] and P. A. Żołnierczuk[10]

(Jefferson Lab Hall A Collaboration)

[1]*California Institute of Technology, Pasadena, California 91125, USA*
[2]*California State University, Los Angeles, Los Angeles, California 90032, USA*
[3]*Université Blaise Pascal Clermont-Ferrand et CNRS/IN2P3 LPC 63, 177 Aubière Cedex, France*
[4]*Florida International University, Miami, Florida 33199, USA*
[5]*Florida State University, Tallahassee, Florida 32306, USA*
[6]*University of Illinois, Urbana, Illinois 61801, USA*
[7]*Istituto Nazionale di Fisica Nucleare, Sezione Sanità, 00161 Roma, Italy*
[8]*Thomas Jefferson National Accelerator Facility, Newport News, Virginia 23606, USA*
[9]*Kent State University, Kent, Ohio 44242, USA*
[10]*University of Kentucky, Lexington, Kentucky 40506, USA*
[11]*University of Maryland, College Park, Maryland 20742, USA*
[12]*University of Massachusetts Amherst, Amherst, Massachusetts 01003, USA*
[13]*Massachusetts Institute of Technology, Cambridge, Massachusetts 02139, USA*
[14]*University of New Hampshire, Durham, New Hampshire 03824, USA*
[15]*Old Dominion University, Norfolk, Virginia 23529, USA*
[16]*Rutgers, The State University of New Jersey, Piscataway, New Jersey 08855, USA*
[17]*CEA Saclay, DAPNIA/SPhN, F-91191 Gif sur Yvette, France*
[18]*Syracuse University, Syracuse, New York 13244, USA*
[19]*University of Tel Aviv, Tel Aviv 69978, Israel*
[20]*Temple University, Philadelphia, Pennsylvania 19122, USA*
[21]*University of Virginia, Charlottesville, Virginia 22904, USA*
[22]*College of William and Mary, Williamsburg, Virginia 23187, USA*
(Received 23 April 2003; published 7 January 2004)

We have measured the neutron spin asymmetry A_1^n with high precision at three kinematics in the deep inelastic region at $x = 0.33$, 0.47, and 0.60, and $Q^2 = 2.7$, 3.5, and 4.8 $(\mathrm{GeV}/c)^2$, respectively. Our results unambiguously show, for the first time, that A_1^n crosses zero around $x = 0.47$ and becomes significantly positive at $x = 0.60$. Combined with the world proton data, polarized quark distributions were extracted. Our results, in general, agree with relativistic constituent quark models and with perturbative quantum chromodynamics (PQCD) analyses based on the earlier data. However they deviate from PQCD predictions based on hadron helicity conservation.

DOI: 10.1103/PhysRevLett.92.012004 PACS numbers: 13.60.Hb, 24.85.+p, 25.30.–c

After over 25 years of experiments measuring nucleon spin structure, it is now widely accepted that the intrinsic quark spin contributes only a small fraction (20%–30%) of the total nucleon spin. The spin sum rule [1] indicates that the remaining part is carried by the quarks and gluons orbital angular momentum (OAM) and gluon spin.

Here we present precise data in a new kinematic region where the Bjorken scaling variable x is large. For these kinematics, the valence quarks dominate and ratios of structure functions can be estimated based on our knowledge of the interactions between quarks. Specifically, in the limit of large Q^2 (the four momentum transfer

squared), the asymmetry A_1(the ratio of the polarized and the unpolarized structure functions g_1/F_1) is expected to approach 1 as $x \to 1$. This is a dramatic prediction, since all previous data on the neutron A_1^n are either negative or consistent with zero. Furthermore, in the region $x > 0.3$, both sea-quark and gluon contributions are small and the physics of the valence quarks can be exposed. Relativistic constituent quark models (RCQM, which include OAM) and leading-order perturbative QCD (PQCD) predictions assuming hadron-helicity-conservation (no OAM) make dramatically different predictions for the proton down-quark polarized distribution in the valence quark region. A more complete QCD calculation, describing OAM at the current-quark and gluon level, might agree with the RCQM description. The connection between these descriptions is of paramount importance to a complete description of the nucleon spin using QCD. Thus, precision data in the valence quark region are crucial to improve our understanding of the nucleon spin.

A_1 is known as the nucleon virtual-photon asymmetry and is extracted from the polarized deep inelastic scattering (DIS) cross sections as $A_1 = (\sigma_{1/2} - \sigma_{3/2})/(\sigma_{1/2} + \sigma_{3/2})$, where $\sigma_{1/2\,(3/2)}$ is the total virtual photoabsorption cross section for the nucleon with a projection of 1/2 (3/2) for the total spin along the direction of photon momentum [2]. At finite Q^2, A_1 is related to the polarized and unpolarized structure functions g_1, g_2, and F_1 through

$$A_1(x, Q^2) = [g_1(x, Q^2) - \gamma^2 g_2(x, Q^2)]/F_1(x, Q^2), \quad (1)$$

where $\gamma^2 = 4M^2x^2/Q^2$, M is the nucleon mass, $Q^2 = 4EE'\sin^2(\theta/2)$, $x = Q^2/(2M\nu)$, E is the beam energy, E' is the energy of the scattered electron, $\nu = E - E'$ is the energy transfer to the target, and θ is the scattering angle in the lab frame. At high Q^2, one has $\gamma^2 \ll 1$ and $A_1 \approx g_1/F_1$. Since g_1 and F_1 follow roughly the same Q^2 evolution in leading-order QCD, A_1 is expected to vary quite slowly with Q^2.

To first approximation, the constituent quarks in the neutron can be described by an SU(6) symmetric wave function [3]

$$\begin{aligned} |n\uparrow\rangle = {} & \frac{1}{\sqrt{2}}|d^{\uparrow}(du)_{0,0,0}\rangle + \frac{1}{\sqrt{18}}|d^{\uparrow}(du)_{1,1,0}\rangle \\ & - \frac{1}{3}|d^{\downarrow}(du)_{1,1,1}\rangle - \frac{1}{3}|u^{\uparrow}(dd)_{1,1,0}\rangle \\ & + \frac{\sqrt{2}}{3}|u^{\downarrow}(dd)_{1,1,1}\rangle, \end{aligned} \quad (2)$$

where u (d) is the wave function of up (down) quark inside the neutron and the subscripts refer to I, S, and S_z, the total isospin, total spin, and the spin projection of the spectator diquark state. In this limit both $S = 1$ and $S = 0$ diquark states contribute equally to the observables of interest, leading to the predictions of $A_1^p = 5/9$ and $A_1^n = 0$.

However, from measurements of the x dependence of the ratio F_2^p/F_2^n in unpolarized DIS [4] it is known that the SU(6) symmetry is broken. A phenomenological SU(6) symmetry breaking mechanism is the hyperfine interaction among the quarks. Its effect on the nucleon wave function is to lower the energy of the $S = 0$ diquark state, allowing the first term of Eq. (2) to be more stable and hence to dominate the high momentum tail of the quark distributions, which is probed as $x \to 1$. In this picture one obtains $\Delta u/u \to 1$, $\Delta d/d \to -1/3$, and $A_1^{n,p} \to 1$ as $x \to 1$, with $\Delta u(\Delta d)$ and $u(d)$ the polarized and unpolarized quark distributions for the $u(d)$ quark in the proton. The hyperfine interaction is often used to break SU(6) symmetry in RCQM to calculate $A_1^n(x)$ and $A_1^p(x)$ in the region $0.4 < x < 1$ [5–7].

In the PQCD approach [8,9] it was noted that the quark-gluon interactions cause only the $S = 1$, $S_z = 1$ diquark states to be suppressed as $x \to 1$, rather than the full $S = 1$ states as in the case for the hyperfine interaction. By assuming zero quark OAM and helicity conservation, it has been shown further that a quark with $x \to 1$ must have the same helicity as the nucleon. This mechanism has been referred to as hadron helicity conservation (HHC) and was used to build parton distribution functions [10] and to fit DIS data [11]. In this approach one has $A_1^{n,p} \to 1$, $\Delta u/u \to 1$, and $\Delta d/d \to 1$ as $x \to 1$. This is one of the few places where QCD can make a prediction for the structure function ratios.

The HHC is based on leading-order PQCD where the quark OAM is assumed to be zero. Recent data on the tensor polarization in elastic $e - {}^2\mathrm{H}$ scattering [12], neutral pion photoproduction [13], and the proton form factors [14,15] are in disagreement with HHC predictions. It has been suggested that effects beyond leading-order PQCD, such as the quark OAM [16–18], might play an important role in processes involving spin flips. Calculations including quark OAM were performed to interpret the proton form factor data [18]. These kinds of calculations may be possible in the future for A_1^n and other observables in the large x region [19].

Other available predictions for A_1^n include those from the bag model [20], the LSS next-to-leading order (NLO) polarized parton densities [21], the chiral soliton model [22], a global NLO QCD analysis of DIS data based on a statistical picture of the nucleon [23], and quark-hadron duality based on three different SU(6) symmetry breaking scenarios [24].

We measured inclusive deep inelastic scattering of longitudinally polarized electrons from a polarized ^{3}He target in Hall A of the Thomas Jefferson National Accelerator Facility. Data were collected at three kinematics, $x = 0.33$, 0.47, and 0.60, with $Q^2 = 2.7$, 3.5, and 4.8 $(\mathrm{GeV}/c)^2$, respectively. The invariant mass squared $W^2 = M^2 + 2M\nu - Q^2$ was above the resonance region.

The parallel ($A_\parallel$) and perpendicular ($A_\perp$) asymmetries were measured. They are defined as

$$A_\parallel = \frac{\sigma^{\downarrow\Uparrow} - \sigma^{\uparrow\Uparrow}}{\sigma^{\downarrow\Uparrow} + \sigma^{\uparrow\Uparrow}} \quad \text{and} \quad A_\perp = \frac{\sigma^{\downarrow\Rightarrow} - \sigma^{\uparrow\Rightarrow}}{\sigma^{\downarrow\Rightarrow} + \sigma^{\uparrow\Rightarrow}}, \qquad (3)$$

where $\sigma^{\downarrow\Uparrow}$ ($\sigma^{\uparrow\Uparrow}$) is the cross section for a longitudinally (with respect to the beam line) polarized target with the electron spin aligned antiparallel (parallel) to the target spin; $\sigma^{\downarrow\Rightarrow}$ ($\sigma^{\uparrow\Rightarrow}$) is the cross section for a transversely polarized target with the electron spin aligned antiparallel (parallel) to the beam direction, and with the scattered electrons detected on the same side of the beam line as that to which the target spin is pointing. One can extract A_1 as

$$A_1 = \frac{A_\parallel}{D(1+\eta\xi)} - \frac{\eta A_\perp}{d(1+\eta\xi)}, \qquad (4)$$

where $D = (1 - \epsilon E'/E)/(1 + \epsilon R)$, $d = D\sqrt{2\epsilon/(1+\epsilon)}$, $\eta = \epsilon\sqrt{Q^2}/(E - E'\epsilon)$, $\xi = \eta(1+\epsilon)/(2\epsilon)$, $\epsilon = 1/[1 + 2(1 + 1/\gamma^2)\tan^2(\theta/2)]$, and R is the ratio of the longitudinal and transverse virtual-photon absorption cross sections σ_L/σ_T [2]. Similarly, the ratio of structure functions is given by $g_1/F_1 = [A_\parallel + A_\perp \tan(\theta/2)]/D'$, with $D' = [(1-\epsilon)(2-y)]/[y(1+\epsilon R)]$ and $y = \nu/E$.

The polarized electron beam was produced by illuminating a strained GaAs photocathode with circularly polarized light. We used a beam energy of 5.7 GeV. The beam polarization of $P_b = (79.7 \pm 2.4)\%$ was measured regularly by Møller polarimetry and was monitored by Compton polarimetry. The beam helicity was flipped at a frequency of 30 Hz. To reduce possible systematic errors, data were taken for four different beam helicity and target polarization configurations for the parallel setting and two for the perpendicular setting.

The polarized ^{3}He target is based on the principles of optical pumping and spin exchange. The target cell is a 25 cm long glass vessel. The in-beam target density was about 3.5×10^{20} ^{3}He/cm^3. The target polarization was measured by both the NMR technique of adiabatic fast passage [25], and a technique based on electron paramagnetic resonance [26]. The average in-beam target polarization was $P_t = (40 \pm 1.5)\%$ at a typical beam current of 12 μA. The product of the beam and target polarizations was verified at the level of $\Delta(P_b P_t)/(P_b P_t) \leqslant 4.5\%$ by measuring the longitudinal asymmetry of $\vec{e} - \overrightarrow{^3\text{He}}$ elastic scattering.

The scattered electrons were detected by the Hall A high resolution spectrometer (HRS) pair [27] at two scattering angles of 35° and 45°. A CO_2 gas Čerenkov detector and a double-layered lead-glass shower counter were used to separate electrons from the pion background. The combined pion rejection factor provided by the two detectors was found to be better than 10^4 for both HRSs, with a 99% identification efficiency for electrons.

The asymmetries are extracted from the data as $A_{\parallel,\perp} = A_{\text{raw}}/(f P_b P_t) + \Delta A^{RC}_{\parallel,\perp}$, where A_{raw} is the raw asymmetry and $f = 0.92 \sim 0.94$ is the target dilution factor due to a small amount of unpolarized N_2 mixed with the polarized ^{3}He gas. Radiative corrections $\Delta A^{RC}_{\parallel,\perp}$ were performed for both the internal and the external radiation effects. Internal radiative corrections were applied using POLRAD2.0 [28], the most up-to-date structure functions, and our data for the neutron polarized structure functions. External radiative corrections were performed based on the procedure first described by Mo and Tsai [29]. The uncertainty in the correction was studied by using various fits [30] to the world data for F_2, g_1, g_2, and R. False asymmetries were checked to be negligible by measuring the asymmetries of polarized e^- beam scattering off an unpolarized ^{12}C target.

From $A_{\parallel,\perp}$ one can calculate $A_1^{^3\text{He}}$ using Eq. (4). A ^{3}He model which includes S, S', D states and preexisting $\Delta(1232)$ component in the ^{3}He wave function [31] was used for extracting A_1^n from $A_1^{^3\text{He}}$. It gives

$$A_1^n = \frac{F_2^{^3\text{He}}[A_1^{^3\text{He}} - 2\frac{F_2^p}{F_2^{^3\text{He}}} P_p A_1^p (1 - \frac{0.014}{2P_p})]}{P_n F_2^n (1 + \frac{0.056}{P_n})}, \qquad (5)$$

where $P_n = 0.86^{+0.036}_{-0.02}$ and $P_p = -0.028^{+0.009}_{-0.004}$ are the effective nucleon polarizations of the neutron and the proton inside ^{3}He [31–33]. We used the latest world proton and deuteron fits [34,35] for F_2 and R, with nuclear effects corrected [36]. The A_1^p contribution was obtained by fitting the world proton data [30]. Compared to the convolution approach [32] used by previous polarized ^{3}He experiments, Eq. (5) increases the value of A_1^n by 0.01–0.02 in the region $0.2 < x < 0.7$, which is small compared to our statistical error bars. Equation (5) was also used for extracting g_1^n/F_1^n from $g_1^{^3\text{He}}/F_1^{^3\text{He}}$ by substituting g_1/F_1 for A_1.

Results for A_1^n and g_1^n/F_1^n are given in Table I. The A_1^n results are shown in Fig. 1. The smaller and full error bars show the statistical and total errors, respectively. The largest systematic error comes from the uncertainties in P_p and P_n.

The new datum at $x = 0.33$ is in good agreement with world data. For $x > 0.4$, the precision of A_1^n data has been improved by about an order of magnitude. This is the first experimental evidence that A_1^n becomes positive at large x. Among all model-based calculations [3,6,10,11,20,22], the trend of our data is consistent with the RCQM predictions [6] which suggest that A_1^n becomes increasingly positive at even higher x. However, they do not agree with the BBS [10] and LSS(BBS) [11] parametrizations in which HHC is imposed. Our data are in good agreement with the LSS 2001 PQCD fit to previous data [21] and a global NLO QCD analysis of DIS data using a statistical picture of the nucleon [23].

TABLE I. Results for A_1^n and g_1^n/F_1^n, Q^2 values are given in $(\mathrm{GeV}/c)^2$, errors are given as $\pm$ statistical $\pm$ systematic.

x	Q^2	A_1^n	g_1^n/F_1^n
0.33	2.71	$-0.048 \pm 0.024^{+0.015}_{-0.016}$	$-0.043 \pm 0.022^{+0.009}_{-0.009}$
0.47	3.52	$-0.006 \pm 0.027^{+0.019}_{-0.019}$	$+0.040 \pm 0.035^{+0.011}_{-0.011}$
0.60	4.83	$+0.175 \pm 0.048^{+0.026}_{-0.028}$	$+0.124 \pm 0.045^{+0.016}_{-0.017}$

Assuming the strange quark distributions $s(x)$, $\bar{s}(x)$, $\Delta s(x)$, and $\Delta\bar{s}(x)$ to be negligible in the region $x > 0.3$, and ignoring any Q^2 dependence, one can extract polarized quark distribution functions based on the quark-parton model as

$$\frac{\Delta u + \Delta\bar{u}}{u + \bar{u}} = \frac{4}{15}\frac{g_1^p}{F_1^p}(4 + R^{du}) - \frac{1}{15}\frac{g_1^n}{F_1^n}(1 + 4R^{du});$$
$$\frac{\Delta d + \Delta\bar{d}}{d + \bar{d}} = \frac{4}{15}\frac{g_1^n}{F_1^n}\left(4 + \frac{1}{R^{du}}\right) - \frac{1}{15}\frac{g_1^p}{F_1^p}\left(1 + \frac{4}{R^{du}}\right),$$

where $R^{du} = (d + \bar{d})/(u + \bar{u})$. We performed a fit to the world g_1^p/F_1^p data [30] and used R^{du} extracted from proton and deuteron structure function data [40]. Results for $(\Delta u + \Delta\bar{u})/(u + \bar{u})$ and $(\Delta d + \Delta\bar{d})/(d + \bar{d})$ extracted from our g_1^n/F_1^n data are listed in Table II.

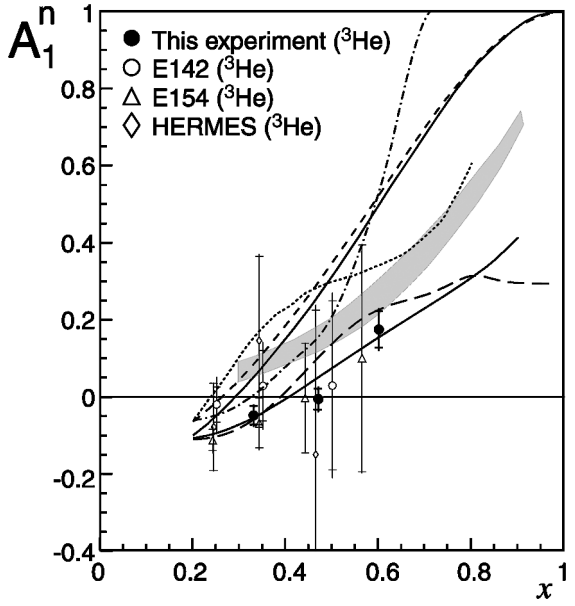

FIG. 1. Our A_1^n results compared with theoretical predictions and existing data obtained from a polarized ^{3}He target [37–39]. Curves: predictions of A_1^n from SU(6) symmetry (zero) [3], constituent quark model (shaded band) [6], and statistical model (long-dashed) [23]; predictions of g_1^n/F_1^n from PQCD HHC based BBS parametrization (higher solid) [10] and LSS(BBS) parametrization (dashed) [11], bag model with the effect of hyperfine interaction but without meson cloud (dash-dotted) [20], LSS 2001 NLO polarized parton densities (lower solid) [21], and chiral soliton model (dotted) [22].

Figure 2 shows our results along with HERMES data [41]. The dark-shaded error band is the uncertainty due to neglecting the strangeness contributions. To compare with the RCQM prediction which is given for valence quarks, the difference between $\Delta q_V/q_V$ and $(\Delta q + \Delta\bar{q})/(q + \bar{q})$ was estimated and is shown as the light-shaded band. Here $q_V(\Delta q_V)$ is the unpolarized (polarized) valence quark distribution for u or d quark. Both errors were estimated using the CTEQ6M [42] and MRST2001 [43] unpolarized parton distribution functions and the positivity conditions that $|\Delta q/q| \leqslant 1$, $|\Delta\bar{q}/\bar{q}| \leqslant 1$, and $|\Delta q_V/q_V| \leqslant 1$. Results shown in Fig. 2 agree well with the predictions from RCQM [6] and LSS 2001 NLO polarized parton densities [21]. The results agree reasonably well with the statistical model calculation [23] but do not agree with the predictions from LSS(BBS) parametrization [11] based on hadron helicity conservation.

In summary, we have obtained precise data on the neutron spin asymmetry A_1^n and the structure function ratio g_1^n/F_1^n in the deep inelastic region at large x. Our data show a clear trend that A_1^n becomes positive at large x. Combined with the world proton data, the polarized quark distributions $(\Delta u + \Delta\bar{u})/(u + \bar{u})$ and $(\Delta d + \Delta\bar{d})/(d + \bar{d})$ were extracted. Our results agree with the LSS 2001 PQCD fit to the previous data and the trend agrees with the hyperfine-perturbed RCQM predictions. The new data do not agree with the prediction from PQCD-based hadron helicity conservation, which suggests that effects beyond leading-order PQCD, such as the quark orbital angular momentum may play an important role in this kinematic region. Extension of precision measurements of A_1^n to higher x and wider Q^2 range is planned with the future JLab 12 GeV energy upgrade.

We would like to thank the personnel of Jefferson Lab for their efforts which resulted in the successful completion of the experiment. We thank S. J. Brodsky, L. Gamberg, N. Isgur, X. Ji, E. Leader, W. Melnitchouk, D. Stamenov, J. Soffer, M. Strikman, A. Thomas, H. Weigel, and their collaborators for the theoretical support and helpful discussions. This work was supported by the Department of Energy (DOE), the National Science Foundation, the Italian Istituto Nazionale di Fisica Nucleare, the French Institut National de Physique Nucléaire et de Physique des Particules, the French Commissariat à l'Énergie Atomique and the Jeffress Memorial Trust. The Southeastern Universities Research

TABLE II. Results for the polarized quark distributions. The three errors are those due to the g_1^n/F_1^n statistical error, g_1^n/F_1^n systematic error and the uncertainties of g_1^p/F_1^p and R^{du} fits.

x	$(\Delta u + \Delta\bar{u})/(u + \bar{u})$	$(\Delta d + \Delta\bar{d})/(d + \bar{d})$
0.33	$0.565 \pm 0.005^{+0.002+0.025}_{-0.002-0.026}$	$-0.274 \pm 0.032^{+0.013+0.010}_{-0.013-0.018}$
0.47	$0.664 \pm 0.007^{+0.002+0.060}_{-0.002-0.060}$	$-0.291 \pm 0.057^{+0.018+0.032}_{-0.018-0.034}$
0.60	$0.737 \pm 0.007^{+0.003+0.116}_{-0.003-0.116}$	$-0.324 \pm 0.083^{+0.031+0.085}_{-0.031-0.089}$

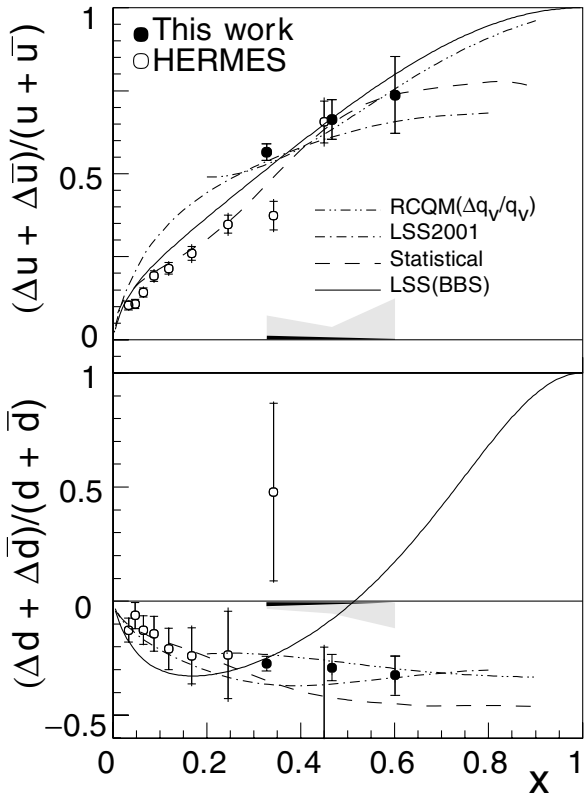

FIG. 2. Results for $(\Delta u + \Delta\bar{u})/(u + \bar{u})$ and $(\Delta d + \Delta\bar{d})/(d + \bar{d})$ in the quark-parton model, compared with HERMES data [41], the RCQM predictions [6], predictions from LSS 2001 NLO polarized parton densities [21], the statistical model [23], and PQCD-based predictions incorporating HHC [11]. The error bars of our data include the uncertainties given in Table II. The dark-shaded error band on the horizontal axis shows the uncertainty in the data due to neglecting s and $\bar{s}$ contributions. The light-shaded band shows the difference between $\Delta q_V/q_V$ and $(\Delta q + \Delta\bar{q})/(q + \bar{q})$ that needs to be applied to the data when comparing with the RCQM calculation.

Association operates the Thomas Jefferson National Accelerator Facility for the DOE under Contract No. DE-AC05-84ER40150.

[1] R. L. Jaffe and A. Manohar, Nucl. Phys. **B337**, 509 (1990); B.W. Filippone and X. Ji, Adv. Nucl. Phys. **26**, 1 (2001).
[2] R. P. Feynman, *Photon Hadron Interactions* (Addison Wesley, Longman, 1972).
[3] F. Close, Nucl. Phys. **B80**, 269 (1974).
[4] R. Carlitz, Phys. Lett. **58B**, 345 (1975); J. Franklin, Phys. Rev. D **16**, 21 (1977).
[5] Z. Dziembowski, C. J. Martoff, and P. Zyla, Phys. Rev. D **50**, 5613 (1994).
[6] N. Isgur, Phys. Rev. D **59**, 034013 (1999).
[7] B.-Q. Ma, Phys. Lett. B **375**, 320 (1996).
[8] G. R. Farrar and D. R. Jackson, Phys. Rev. Lett. **35**, 1416 (1975).
[9] G. R. Farrar, Phys. Lett. **70B**, 346 (1977).
[10] S. J. Brodsky, M. Burkardt, and I. Schmidt, Nucl. Phys. **B441**, 197 (1995).
[11] E. Leader, A.V. Sidorov, and D. B. Stamenov, Int. J. Mod. Phys. A **13**, 5573 (1998).
[12] D. Abbott *et al.*, Phys. Rev. Lett. **84**, 5053 (2000).
[13] K. Wijesooriya *et al.*, Phys. Rev. C **66**, 034614 (2002).
[14] M. K. Jones *et al.*, Phys. Rev. Lett. **84**, 1398 (2000).
[15] O. Gayou *et al.*, Phys. Rev. Lett. **88**, 092301 (2002).
[16] G. A. Miller and M. R. Frank, Phys. Rev. C **65**, 065205 (2002).
[17] R.V. Buniy, P. Jain, and J. P. Ralston, in *Intersections of Particle and Nuclear Physics—2000*, AIP Conf. Proc. No. 549 (AIP, New York, 2000), p. 302.
[18] A.V. Belitsky, X. Ji, and F. Yuan, Phys. Rev. Lett. **91**, 092003 (2003); X. Ji, J.-P. Ma, and F. Yuan, Nucl. Phys. **B652**, 383 (2003).
[19] X. Ji (private communication).
[20] C. Boros and A.W. Thomas, Phys. Rev. D **60**, 074017 (1999); F. M. Steffens and A.W. Thomas (private communication).
[21] E. Leader, A.V. Sidorov, and D. B. Stamenov, Eur. Phys. J. C **23**, 479 (2002).
[22] H. Weigel, L. Gamberg, and H. Reinhardt, Phys. Lett. B **399**, 287 (1997); Phys. Rev. D **55**, 6910 (1997).
[23] C. Bourrely, J. Soffer, and F. Buccella, Eur. Phys. J. C **23**, 487 (2002).
[24] F. E. Close and W. Melnitchouk, Phys. Rev. C **68**, 035210 (2003).
[25] A. Abragam, *Principles of Nuclear Magnetism* (Oxford University, New York, 1961).
[26] M.V. Romalis and G. D. Cates, Phys. Rev. A **58**, 3004 (1998).
[27] J. Alcorn *et al.*, Nucl. Inst. Meth. (to be published).
[28] I. Akushevich *et al.*, Comput. Phys. Commun. **104**, 201 (1997).
[29] L. Mo and Y. Tsai, Rev. Mod. Phys. **41**, 205 (1969).
[30] X. Zheng, Ph.D. thesis, M.I.T., 2002.
[31] F. Bissey *et al.*, Phys. Rev. C **65**, 064317 (2002).
[32] C. Ciofi degli Atti, S. Scopetta, E. Pace, and G. Salmè, Phys. Rev. C **48**, R968 (1993).
[33] A. Nogga, Ph.D. thesis, Ruhr-Universität Bochum, 2001.
[34] M. Arneodo *et al.*, Phys. Lett. B **364**, 107 (1995).
[35] K. Abe *et al.*, Phys. Lett. B **452**, 194 (1999).
[36] W. Melnitchouk and A.W. Thomas, Acta Phys. Pol. B **27**, 1407 (1996).
[37] P. L. Anthony *et al.*, Phys. Rev. D **54**, 6620 (1996).
[38] K. Abe *et al.*, Phys. Rev. Lett. **79**, 26 (1997); Phys. Lett. B **405**, 180 (1997).
[39] K. Ackerstaff *et al.*, Phys. Lett. B **404**, 383 (1997).
[40] W. Melnitchouk and A.W. Thomas, Phys. Lett. B **377**, 11 (1996).
[41] K. Ackerstaff, *et al.*, Phys. Lett. B **464**, 123 (1999).
[42] J. Pumplin *et al.*, J. High Energy Phys. **07**, 012 (2002).
[43] A. D. Martin, R. G. Roberts, W. J. Stirling, and R. S. Thorne, Eur. Phys. J. C **23**, 73 (2002).